

ORIGINAL ARTICLE

Aerodynamic Effect of Wing Mirror Usage on the Solaris 7 Solar Car and Demobil 09 Electric Vehicle

T. Batuhan Korkut and Aytac Gören*

Department of Mechanical Engineering, Automatic Control and Robotic Labs, Dokuz Eylul University, 35400 Buca, Izmir, Turkey
Phone: +902323019233

ABSTRACT – This study focuses on the aerodynamic performances of two vehicles by Dokuz Eylul University Solaris Solar Car Project Team. The first vehicle (S7) is a solar-powered vehicle that is designed for World Solar Challenge and the second (D9) is an electric vehicle which is designed for Tubitak EV Challenge. Both vehicles are manufactured using polymer composites and challenged in mentioned races. In this research, a formal optimisation technique based on computational fluid dynamics (CFD) is used to determine the efficient aerodynamic structures under various scenarios. Results clearly show that strategists of the racing teams should take into account the aerodynamic structure of the racing car. Especially before the races which based on efficiency, the apex line is determined, and mirrors should be replaced by back view camera.

ARTICLE HISTORYRevised: 10th Feb 2020Accepted: 27th Mar 2020**KEYWORDS***Aerodynamics;*
Computational fluid
dynamics; *Solar car;*
Electric vehicle; *Power*
consumption

INTRODUCTION

Aerodynamics is the study of how gases interact with moving bodies. Solar-powered and electric vehicles have fewer energy sources or capacities than internal combustion engine vehicles radically. Therefore, the aerodynamic drag coefficient of solar-powered and electric vehicles should be less than the internal combustion engine automobiles. The Solaris 7 solar car requires only 1.845 kW to cruise at 100 km/h, while an internal combustion engine vehicle with drag coefficient value 0.32 requires as much as 13.52 kW [1]. The aerodynamics affects the fuel consumption, handling characteristics, acceleration properties and performance of the car [2, 3, 4, 5, 14]. As fossil fuels are consumed, the aerodynamic design of the vehicle becomes more important. Also, the cooling system, like the system of the brake system cooling is related to aerodynamics. Vehicles have a part that covers the rear wheels in the 1940s. It enables to reduce drag force. At the same time, however, it causes the brake disk temperature to increase. Because of this situation, more aerodynamic rims are preferred instead of covers.

In the past, the first cars were not so different from sharp-edged shapes. Still, today, radical changes have been implemented, analysis techniques have been developed, and their aerodynamic characteristics are improved. In the 1930s, the analyses had been performed by aluminium powder tests and old wind tunnels. Today, these analyses are performed by many sensors implemented wind tunnels, simulation, and analysis software. The aerodynamic design of vehicles changes depending on the result of analyses [14].

When the car travels at high speed, the aerodynamic character of the car is determined. As shown in the sixteenth equation, the drag force caused by gases increases proportionally to the square of the velocity. A car at a speed of 90 km/h consumes 53% of its fuel to overcome the forces of drag resistance [26]. The car spends 30 % of its power to defeat wheels friction force. At least 17% of the power overcome other resistive forces to the motion [8, 11].

As far as this case is concerned, the importance of aerodynamics is understood once again. Solar and electric vehicles are wheeled motor vehicles used for transportation. Most definitions of the vehicle are running primarily on roads, one seat to six seats, have four tires, and mainly transport people rather than goods. The main difference between a mass production ICE vehicle & an EV is that an EV uses an electric motor powered generally by batteries. When solar cars are being charged, they use solar energy whereas when the electric cars are being charged, they use electricity produced in power plants. The design of solar and electric vehicles has some significant points. These are efficient aerodynamic bodies, have lightweight chassis and use extremely efficient systems. Using electric vehicles is getting common day by day. Electric vehicles are more efficient, comfortable in means of vibration, environment-friendly and quiet. However, the use of solar cars is not common yet because the cost of photovoltaics is still expensive.

World Solar Challenge is the world's most prestigious solar car challenge which was started in the year 1987, in which there are 38 universities from 18 different countries. It is held between Darwin and Adelaide in Australia. Solar cars struggle with the lateral wind in the middle region of the Australia continent during the race. The lateral wind that has 45-60 km/h speed causes many accidents. On the other hand, in circuit races, the direction of the vehicle changes instantaneously. Thus, the lateral wind is an important point of the design of solar and electric vehicles participate in the challenge [14,16]. The purpose of this study is to assess the aerodynamics of a solar car and an electric vehicle that is designed and manufactured for solar and efficiency challenges. Besides, investigating moments of various yaw angles according to race circuits. We anticipate that the results lead to new designs.

Altinisik et al. performed an aerodynamic analysis of the one-fifth scale passenger model. They determined and verified various cases about yawing angles and two-vehicle platoons. Authors have concluded that the realisable k-epsilon turbulence model was successful in modelling flows around a passenger car at higher yaw angles and two-vehicle platoon [13].

Bello-Millian et al. determined Ahmed’s body drag coefficient for different yaw angles. During this study, they specified that the connection between the roof and the rear slant angle influence three critical regions about the drag coefficient. In addition, they found that the drag coefficient increases with the yaw angle [4].

Martin Olsson [32] has determined the most efficient mirror structure for the ground vehicle. He decided a combination of wind tunnel testing and CFD simulations are necessary to find a good mirror design. The result from smaller changes (1-2 drag counts difference) cannot be trusted. Only with larger changes, drag counts difference, can the results be considered trustworthy. Onur Yemenici [33] found that the static pressures were not uniformly distributed over the rearview side mirror, and the pressure coefficients took minimum values at the separation points of the boundary layer from the mirror surface.

COMPUTATIONAL DOMAIN

Solar and electric vehicle models are designed in SOLIDWORKS 2016 software, and computational fluid dynamics analyses are simulated in ANSYS Fluent V18.2 software. Dimensions and properties of solar and electric vehicles are given in Table 1. Computational domain dimensions of the problem showed in Figure 1 [14, 15, 16, 21, 22]. Boundary conditions of the problem were explained in Table 1. The bodies of the vehicle and lateral walls are defined as stationary wall and the shear conditions no-slip. The entrance of the computational domain is defined as the velocity-inlet, and the velocity specification method is defined as components. The exit surface of the computational domain is defined as a pressure-outlet. The backflow reference frame is determined as absolute and gauge pressure is 0 Pa.

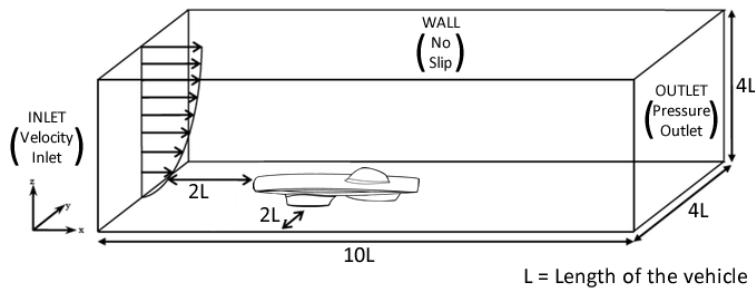


Figure 1. Presentation of the computational domain of flow around the solar and electric vehicles.

Table 1. Dimensions of the computational domain and boundary conditions.

Computational domain			
	Length (m)	Width (m)	Height (m)
Solaris 7	46.0	9.2	9.2
Demobil 09	33.0	6.6	6.6
Boundary conditions			
Boundary	Boundary type	Value	
Inlet	Velocity inlet	33 m/s	
Outlet	Pressure outlet	0 Pa	
Vehicle surface	Stationary wall	No Slip	
Wall	Stationary wall	No Slip	

Table 2. Technical information of Solaris 7 solar car and Demobil 09 electric vehicle.

	Solaris 7	Demobil 09
Length [m]	4.6	3.3
Width [m]	1.8	1.5
Height [m]	1.2	1
Number of wheels	3	4
Body and chassis	Carbon fiber	Carbon fiber
Weight [kg]	175	250

Mesh Generation

When Figure 2 is examined, the differences between the two analyses which have a different mesh structure are exactly seen. This study is called mesh independence. At the end of this study, the optimum structure and solving-time were determined. Due to graphs, the accuracy result was obtained after the set-up, which has 2.65 m mesh number. The structure which has 3.2 m mesh number was determined for optimum solving-time and more accurate results. At the end of this study, twelve computational fluid dynamics problems were solved in efficient and accurate way.

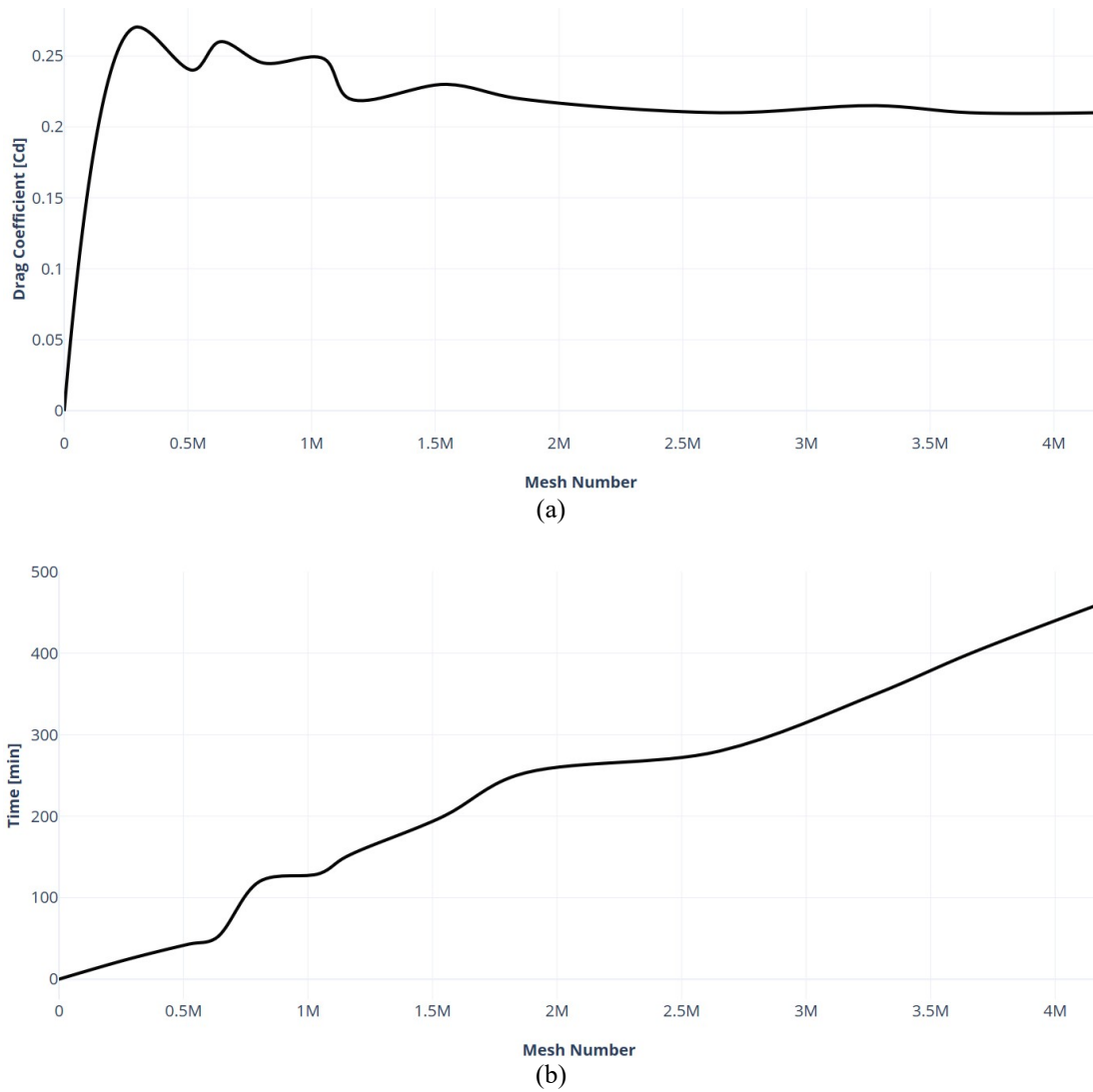


Figure 2. The values of drag coefficients and time duration of analyses that depend on mesh number.

Numerical Approach

Turbulence model

Standard K-epsilon (k-ε) turbulence model is the most common model that is used in CFD to simulate mean flow characteristics for turbulent flow conditions. The flow is assumed fully defined turbulent. The effects of molecular viscosity are negligible. So k- ε turbulent model becomes suitable for turbulent flow. [6,28,29]. Compared with wind tunnel tests, the standard k-epsilon turbulence module has more similar results [6].

It includes two-equation model which transport equations to represent the turbulent properties of the flow [28,29]. The first transported variable is turbulent kinetic energy (k) and the second one transported variable is turbulent dissipation (ε). For turbulent kinetic energy (k),

$$\frac{\partial}{\partial t} (\rho k) + \frac{\partial}{\partial x_i} (\rho k u_i) = \frac{\partial}{\partial x_j} \left[\left(\mu + \frac{\mu_t}{\sigma_k} \right) \frac{\partial k}{\partial x_j} \right] + P_k + P_b - \rho \epsilon - Y_M + S_k \tag{1}$$

For dissipation (ε)

$$\frac{\partial}{\partial t} (\rho \epsilon) + \frac{\partial}{\partial x_i} (\rho \epsilon u_i) = \frac{\partial}{\partial x_j} \left[\left(\mu + \frac{\mu_t}{\sigma_\epsilon} \right) \frac{\partial \epsilon}{\partial x_j} \right] + C_{1\epsilon} \frac{\epsilon}{k} (P_k + C_{3\epsilon} P_b) - C_{2\epsilon} \rho \frac{\epsilon^2}{k} + S_\epsilon \tag{2}$$

Conservation of mass

The conversation of mass is one of the most important and useful equations in fluid dynamics. It allows us to determine if a given flow field conserves mass, and is therefore physically possible. In vector form, the equation is given by,

$$\frac{\partial \rho}{\partial t} + \nabla \cdot (\rho \vec{v}) = S_m \tag{3}$$

The vector form of the conservation of mass is indicated in Eq. (3). It is suitable for incompressible and compressible flows. S_m is any defined sources by user. The continuity equation which is required for 2D axis-symmetric coordinates as in Eq. (4) where v_x and x are on the axial coordinate and v_r and r are on the radial velocity.

$$\frac{\partial \rho}{\partial t} + \frac{\partial}{\partial x} (\rho v_x) + \frac{\partial}{\partial y} (\rho v_r) + \frac{\rho v_r}{r} = S_m \tag{4}$$

Conservation of momentum

The equation for the conservation of linear momentum is obtained by applying Newton’s second law. The net force which acts on the fluid particle is equal to the time rate of change of the linear momentum of the fluid particle [23].

$$\frac{\partial}{\partial x_i} (\rho u_i u_j) = - \frac{\partial p}{\partial x_i} + \frac{\partial}{\partial x_j} \left[\mu \left(\frac{\partial u_i}{\partial x_j} + \frac{\partial u_j}{\partial x_i} - \frac{2}{3} \delta_{ij} \frac{\partial u_l}{\partial x_l} \right) \right] + \frac{\partial}{\partial x_j} (-\rho \overline{u_i u_j}) \tag{5}$$

Drag force

Air flows over the surface of the body of the car during motion. Distribution of pressure changes this relative motion. The external flow also applies a retarding tangential friction force over the surface of the vehicle. The sum of total external and internal retarding forces is called as drag force which is a resistance force [12, 23, 24]. Drag force can be calculated as:

$$F_d = \frac{1}{2} \rho A V^2 C_d \tag{6}$$

Relative airflow approaching the car is at zero yaw angle. The air at the car’s surface moves at zero speed relative to that surface. However, when the air moves away from the surface, the speed of the air approaches to the relative speed of the surrounding air. The area between the point where speed is zero and the point where speed is the relative speed of the surrounding air is called a boundary layer. The boundary layer becomes thicker as an approach from the front of the car to the end. Also, this area contains a velocity gradient. The velocity gradient is related to viscosity. Hence, the air applies a retarding frictional force to the surface of the vehicle. So, friction force increases as the speed of the vehicle increases.

When the flow contacts the surface, the boundary layer is formed. The flow moving relative to each other without velocity components that cross to their motion in the first stage. Therefore, the flow is called laminar. Any actual surface can be fully smooth, so the flow that moving to the opposite direction of motion of the car meets a small bump on the surface. The flow may be deflected from its line, but the viscous friction of the other air particles keeps the flow in its line. Concurrently, when the air particle glances off the small bump, air particles gain momentum away from the surface. And then an impulsive force is applied. At the next hit, the thickening of the boundary layer becomes expanded. Thus the small waves appear and then increase. Lastly, the boundary layer transition to turbulence.

As shown in Table 3 and Eq. (6), the resistive drag force increases as the front cross-sectional area of vehicle increases. In Table 3, shown different vehicle types and their ($C_d \times A$) values. If Eq. (6) is examined, the circumstances which increase the drag force are front sectional area, drag coefficient, and velocity. The drag force which acts on a vehicle is increased as the cross-sectional area of the vehicle increases. This situation is expressed in Eq. (6). With this situation, the shape of the vehicle is a significant part of the aerodynamic structure. Because the drag coefficient is depending on the shape of the vehicle, consequently, the shape of the vehicle affects the drag coefficient. In order to compare the values of aerodynamic resistances of different vehicles Table 2 can be used. In Table 3, $C_D \times A$ values of different shaped vehicles and the vehicles in this research are compared.

Table 3. Different vehicle types and their $C_D \times A$ values.

#	Vehicle	Area	$C_D \times A$
A	Bus	7.62	4.572
B	Car	2.432	0.7296
C	Truck	11.08	8.5980
D	S7 Solar Car	1.07	0.1432
E	D09 EV	1.39	0.2766

Drag coefficient at yaw angle

The aerodynamic drag coefficient which acting on the vehicle is described below:

$$C_d = \frac{F_d}{\frac{1}{2} [\rho A (U_\infty \cos \gamma)^2]} \tag{7}$$

Where ρ is the density of air, A is the cross-sectional area of the vehicle, γ is the yaw angle, F_d is the drag force along the direction of travel, U_∞ is the velocity of the vehicle. [14] The results of drag coefficients that depend on the yaw angle of Demobil 09 and Solaris 7 is introduced in section three.

Power

The power needed to push an object through a fluid increases as the cube of the velocity. A car cruising on a highway at 80 km/h may require only 7.5 kW to overcome air drag, but that same car at 160 km/h requires 60 kW. [17] With a doubling of speed, the drag force quadruples per the formula. Exerting four times the force over a fixed distance produces four times as much work. At twice the speed the work is done twice as fast. Since power is the rate of doing work, four times the work is done in half the time requires eight times the power [12, 24]. The power required to overcome the aerodynamic drag is given by:

$$P = \frac{1}{2} \rho A V^3 C_d \tag{8}$$

Lift force

Lift is the force that is perpendicular to the direction of the car. Lift force is a result of differences of pressure. It depends on speed of the car, density of air, shape of the car and angle of attack [12,24]. Lift force calculated as:

$$F_L = \frac{1}{2} \rho A V^2 C_L \tag{9}$$

CFD analysis

Numerical flow analysis was carried out in ANSYS Fluent® program and computer with features of Intel® Core(TM) i7 4700HQ CPU, 3.40 GHz processor and 12 GB ram. The analyses are made in 33 m/s.

Cross Wind

There has been a lot of wind-induced accidents since transportation services are started. Critical crosswinds towards the travelling vehicle on the road is a significant factor for stability. A critical wind velocity of the overturning of a vehicle depends on the aerodynamic forces caused by crosswinds. The value of critical wind velocity of overturning can be obtained from the equation of the static balance of the action of the external force on the vehicle and aerodynamic characteristics of the vehicle.

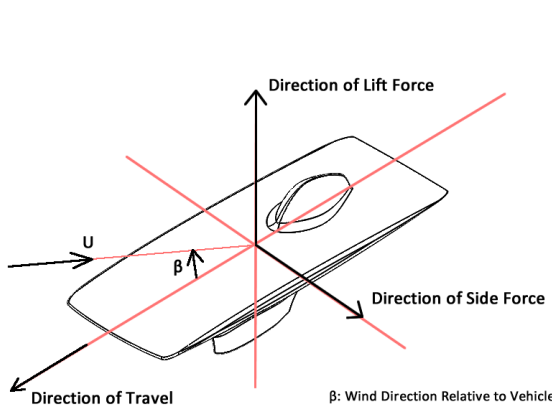


Figure 3. Aerodynamics forces, moments and axes of coordinates fixed to Solaris 7.

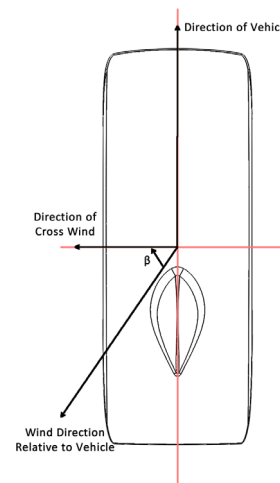


Figure 4. Wind direction of relative to vehicle.

In Figure 3 and Figure 4, the components of the aerodynamic forces on Solaris 7 and wind direction angle are shown. As indicated above, crosswind affects the static balance of the vehicle and aerodynamic forces on the vehicle. In Table 4 the maximum wind gusts in Coober Pedy, South Australia during World Solar Challenge 2017 are shown. Solar teams that participated World Solar Challenge 2017 arrived at Coober Pedy on 11 and 12 October 2017. Maximum wind gusts which on 11 and 12 October are 63 km/h and 33 km/h. These values are critical for solar cars and electric vehicles.

Table 4. Daily weather observations of Coober Pedy, South Australia (October 2017) [27].

Date	Day	Temperature (°C)		Max. wind gust	
		Min	Max	Speed (km/h)	Local time
10	Tu	16	32.5	63	14:53
11	We	18.2	28.3	63	14:49
12	Th	9.9	25.5	33	23:28
13	Fr	11.9	26.9	39	12:08

Yaw Angle

Efficiency is very important in solar-powered and electric vehicle races. Energy capacities and consumption are optimised to run the last part of the capacity to finish the last part of the challenges. For this reason, the apex is an important factor for race cars. For Circuit de Zolder, in which European Solar Challenge is organised, the race car travels at a yaw angle of 15 and 30 degrees at the time of cornering for protecting the apex line. Because of that reason, yaw angles are also varied in the analysis according to various circumstances.

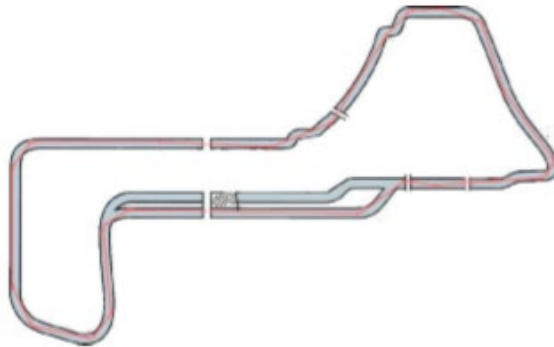


Figure 5. Apex line of the Circuit de Zolder.

NUMERICAL ANALYSIS

CFD Analysis of Demobil 09

Drag coefficient values change according to the yaw angles. For this reason, aerodynamic power consumption is not constant. In this section, the aerodynamic power consumption values of the electric vehicle are analysed according to the crosswind, mirror and mirrorless situations.

Yaw Angle

The drag coefficient was expected to increase with increasing yaw angle. Nonetheless, the total drag force (F_D) on the model axis was also decreasing significantly. Therefore, the reduction in the model drag force and power consumption was observed after the critical yaw angle. The critical yaw angle was determined by 45° as shown in Figure 6.

Figure 6 and Table 5 show the comparison of the measured and the calculated drag force coefficients at increasing yaw angles. Numerical studies showed that the maximum drag coefficient was obtained at a yaw angle of 60° . After 45° , the power consumption started to decrease due to the total drag force reduction. As shown in Figure 7, Figure 8 and Table 6, the pressure difference can be seen on the connection of the roof and slant angle. The critical area of the body was determined the connection of the roof and slant angle. The pressure difference on this area can be examined at various yaw angles.

Table 5. Drag coefficients, force and power consumption values according to the yaw angles.

Wind Speed (m/s)	Parameter	Yaw angle (°)				
		0	15	30	45	60
33.0	C_D	0.1993	0.3032	0.5868	1.3336	1.76
	Drag force (N)	185.35	263.12	409.31	620.13	409.38
	Power (kW)	6.12	8.38	11.69	14.47	6.751

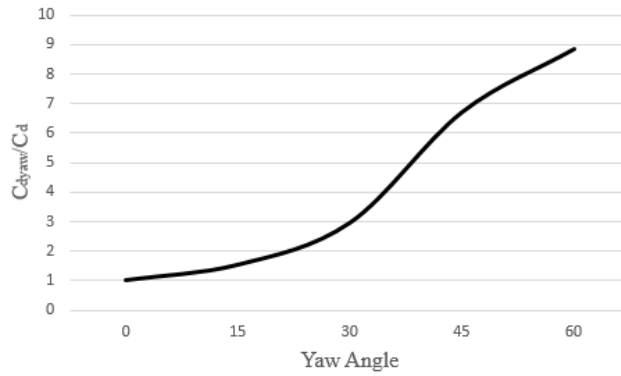


Figure 6. Comparison of the drag coefficient with increasing yaw angles γ at 33 m/s.

The length of the road bend of the Circuit de Zolder is 0.75 km. When Demobil 09 passes the road bends. It consumes 0.0778 kW. If the aerodynamic structure of Demobil 09 doesn't deteriorate, Demobil 09 consume 0.0383 kW. Consequently, each lap has an energy gain of 0.0342 kW. The importance of conservation of aerodynamic structure on road bends can be seen.

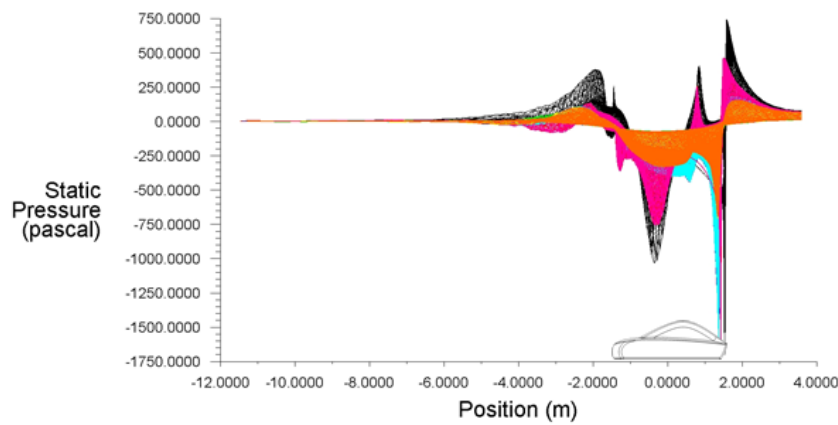


Figure 7. Pressure distribution of Demobil 09 electric vehicle at 0 yaw angle.

Table 6. Pressure distribution and the difference between yaw angles.

Wind speed (m/s)	Position (m)	Yaw angles (°)				
		0	15	30	45	60
33.0		Pressure difference (MPa)				
	-1.5	1.65	0.60	0.50	0.55	0.30
	-1	0.80	0.25	1.95	0.50	0.35
	-0.5	0.40	0.85	0.85	1.10	1.00
	0	0.60	0.55	2.25	1.25	0.75
	0.5	1.00	1.30	1.00	1.35	1.15
	1	0.25	1.85	3.25	2.55	0.60
1.5	0.40	1.75	1.45	0.20	0.20	



(a) 0°



(b) 15°

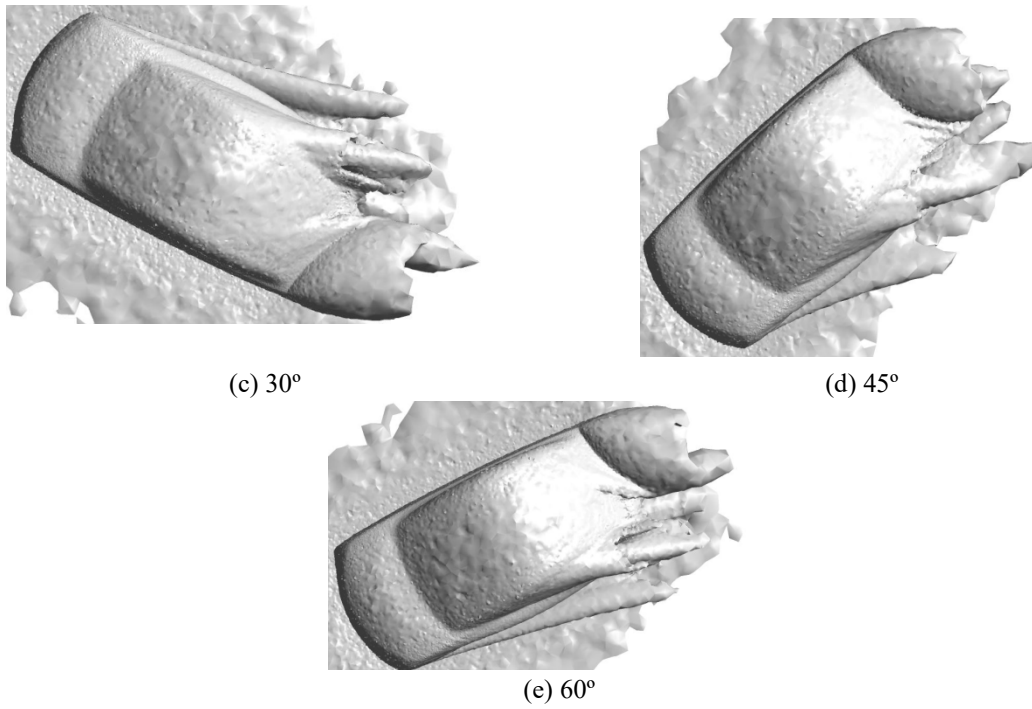


Figure 8. Vortex core regions depend on yaw angles.

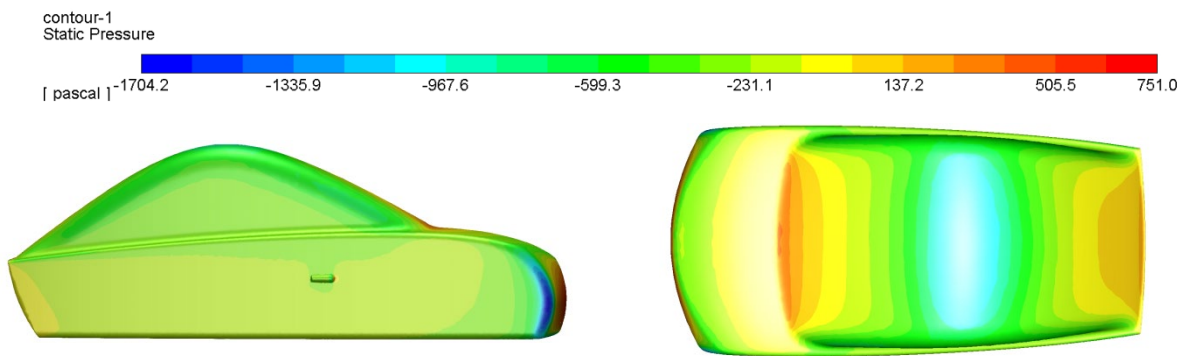
Mirror and camera usage

The effect of mirror usage on vehicles is a critical factor for aerodynamic structure of vehicles. The camera, which shows rearward of the vehicle, is preferred to mirror on new concept vehicles. But, energy consumption on an electric vehicle is important. In this case, these two cases are compared due to energy consumption per one hour. The results of these conditions are shown in Table 7.

Table 7. Comparison of the drag coefficient, drag force and power with wing mirrors and the cover part of rearview camera.

Wind Speed (m/s)	Parameters		Value
33.0	Mirror	Drag coefficient	0.24
		Drag force (N)	233.0
		Power (kW)	7.37
	Camera	Drag coefficient	0.21
		Drag force (N)	195.0
		Power (kW)	6.44

According to the results, due to the pressure build-up in front of and behind the mirror, the air passed into the turbulent flow through the laminar. In this circumstance, the drag coefficient and the power which is consumed increased. When compared to camera and mirror use, camera usage is more efficient than mirror use. The pressure distribution are shown in Figure 9 and Figure 10.



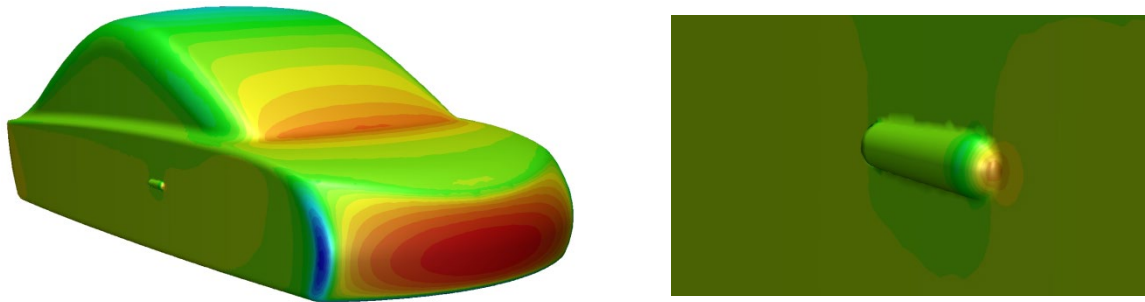


Figure 9. Pressure distribution on Demobil 09 with camera.

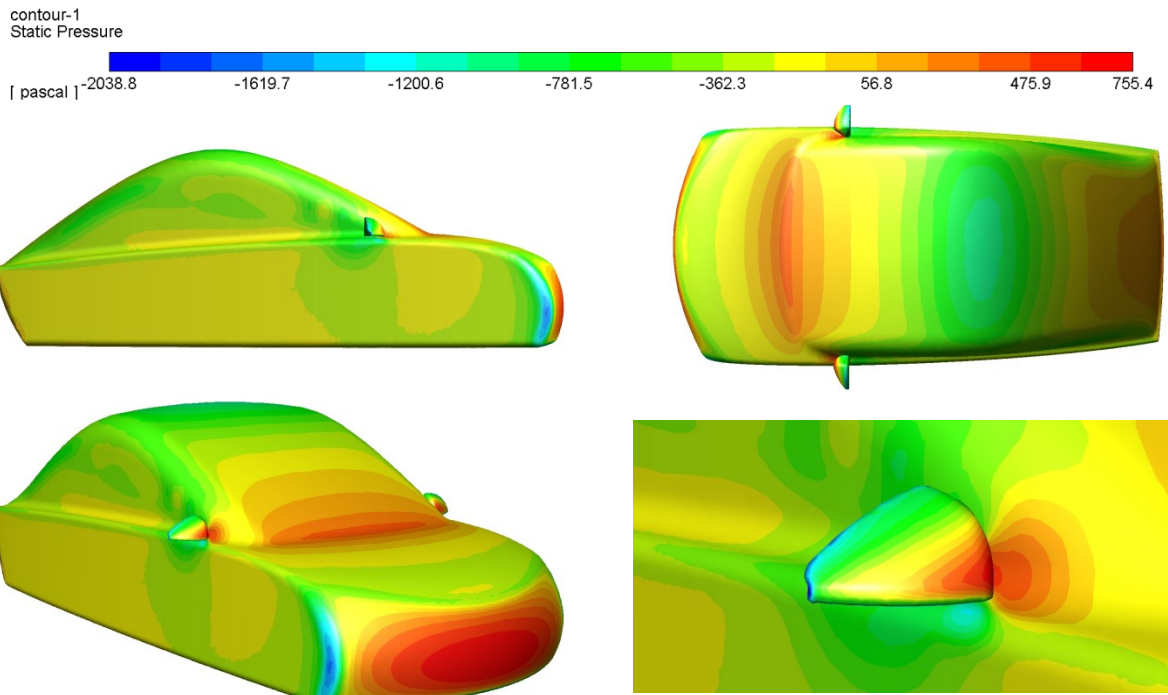


Figure 10. Pressure distribution on Demobil 09 with mirror.

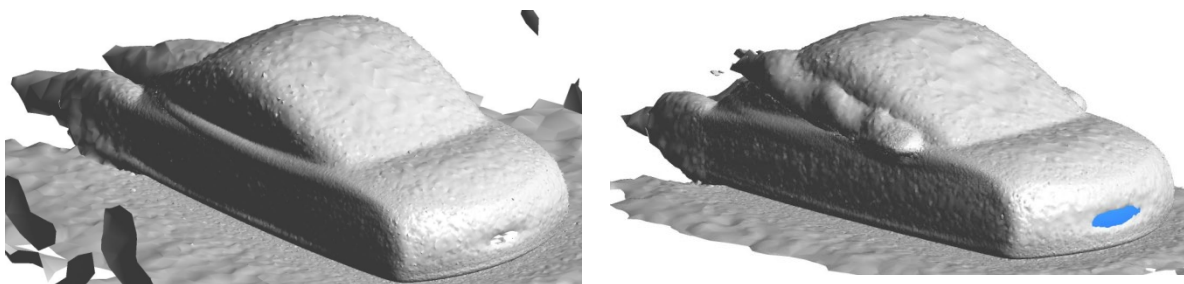


Figure 11. Vortex core regions.

Numerical Analysis Result of Solaris 7

Yaw angle

As indicated in Table 8, the changes in drag coefficient when the vehicle passes bends of roads. So, the values of consumption of vehicle aren't constant when it is on the road. In this section, the effect of crosswind, yaw angles and the usage of camera and mirror on the Solaris 7.

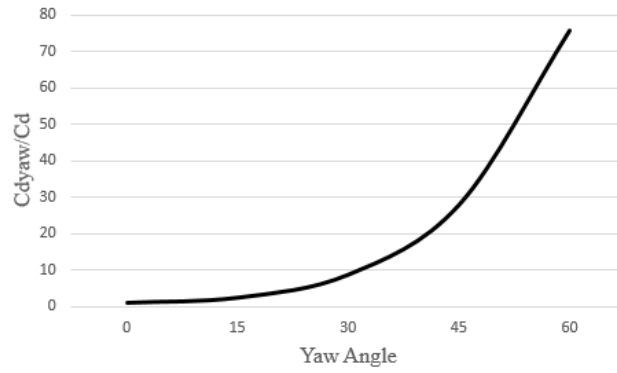


Figure 12. Comparison of the drag coefficient with increasing yaw angles γ at 33 m/s.

Table 8. Comparison of the drag coefficient, drag force and power with increasing yaw angles at 33 m/s.

Wind speed (m/s)	Parameters	Yaw angles (°)				
		0	15	30	45	60
33.0	C_D	0.0919	0.2213	0.8017	2.5592	6.9542
	Drag force (N)	57.7810	129.662	377.672	803.709	1091.96
	Power (kW)	1.904	4.133	10.79	18.75	18.02

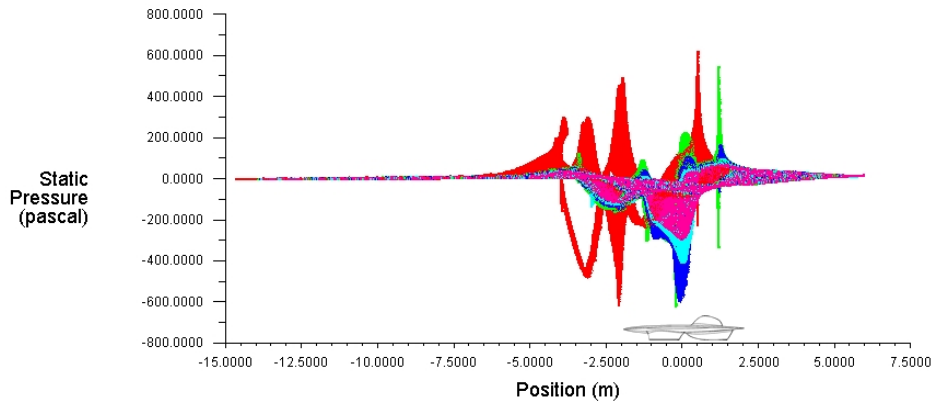
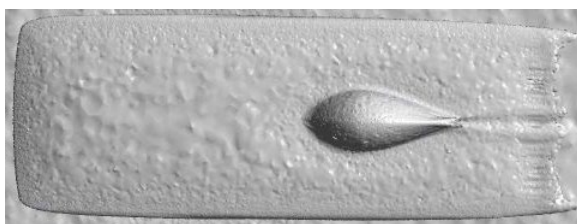


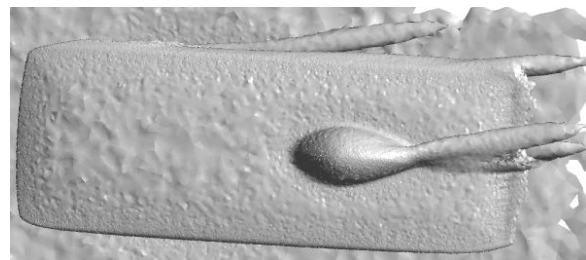
Figure 13. Pressure distribution of Solaris 7 solar car at 0 yaw angle.

Table 9. Pressure distribution and the difference between yaw angles.

Wind speed (m/s)	Position (m)	Yaw angle (°)				
		0	15	30	45	60
33.0		Pressure difference (MPa)				
	-2.3	1.30	0.45	0.33	0.40	0.20
	-1.5	0.30	0.15	1.54	0.46	0.31
	-0.5	0.20	0.47	0.64	0.86	0.78
	0	0.60	0.42	1.86	0.93	0.68
	0.5	0.75	0.95	0.82	0.93	0.89
	1.5	0.90	1.81	2.84	2.25	1.34
2.3	0.10	0.84	0.71	0.37	0.46	



(a) 0°



(b) 15°

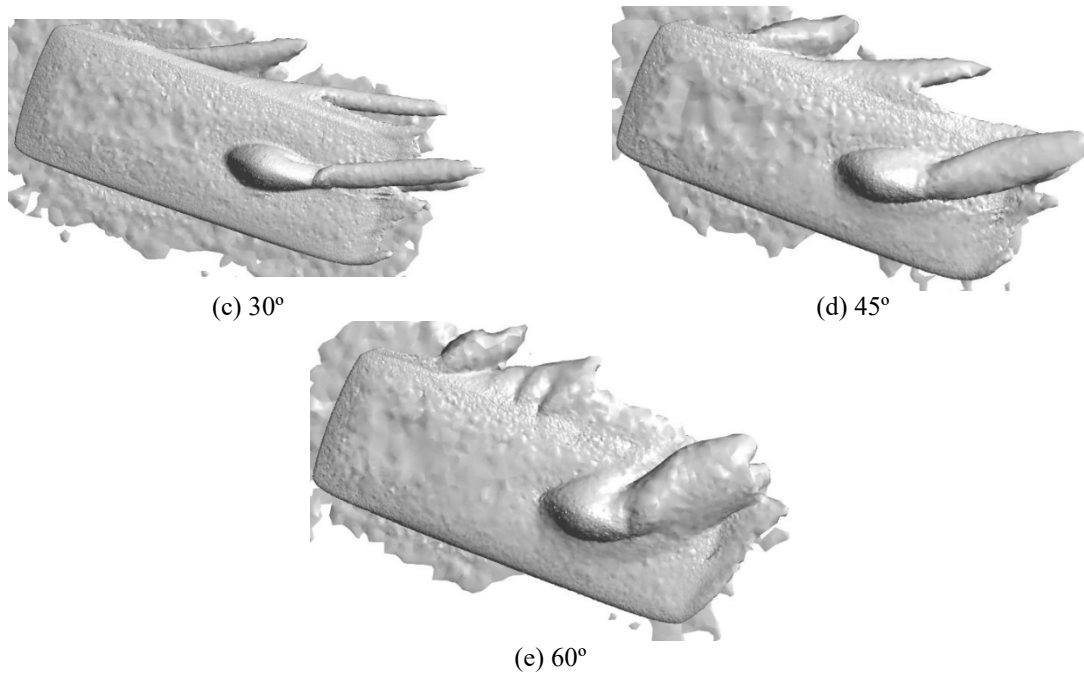


Figure 14. Vortex core regions depend on yaw angles.

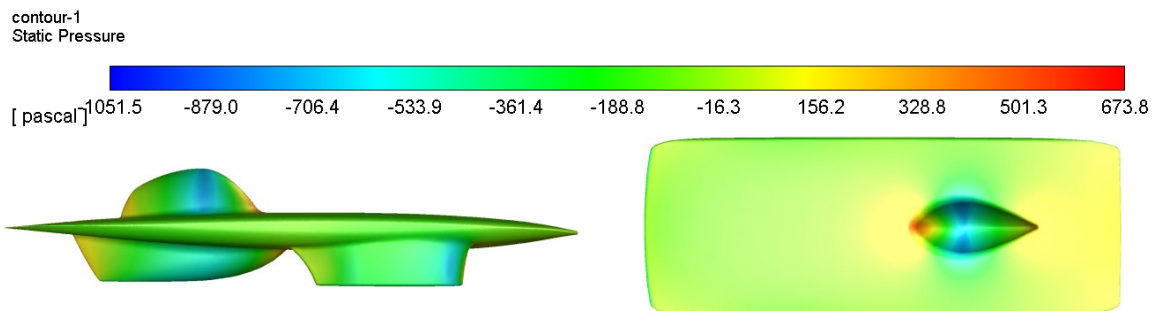
Mirror and camera usage

Conditions which include mirror, camera are examined for developing the aerodynamic structure of Solaris 7. When the Solaris 7 doesn't have a mirror and a camera, its drag coefficient is 0.0919. When it has side mirrors, the drag coefficient of Solaris 7 is 0.13. When it has a camera, the drag coefficient of Solaris 7 is 0.1137. In this case, the energy consumption is getting increased parallel to the drag coefficient. The values of drag forces and energy consumptions are shown in Table 10. Using wing mirrors on Solaris 7 solar car increased the drag coefficient by 42%, and the back-view camera on Solaris 7 solar car increased the drag coefficient by 23.72%. Martin Olsson [32] calculated that the use of mirrors increased the drag coefficient by 51.15% in the CFD and wind tunnel analyses he conducted in his study. In our study, this value is around 45%.

Table 10. Comparison of the drag coefficient, drag force and power with mirror and the cover part of rearview camera.

Wind speed (m/s)	Parameter	Value	
33.0	Mirror	Drag coefficient	0.1305
		Drag force (N)	81.98
		Power (kW)	2.69
	Camera	Drag coefficient	0.1137
		Drag force (N)	71.388
		Power (kW)	2.36

According to results, due to the pressure build-up in front of and behind the mirror, the air passes into the turbulent flow through the laminar. In this circumstances, the drag coefficient and the power which is consumed are increased. Compared to camera and mirror use, it is obviously seen that camera use is more efficient than mirror use. The pressure distributions for the results are shown in Figure 15 to Figure 17.



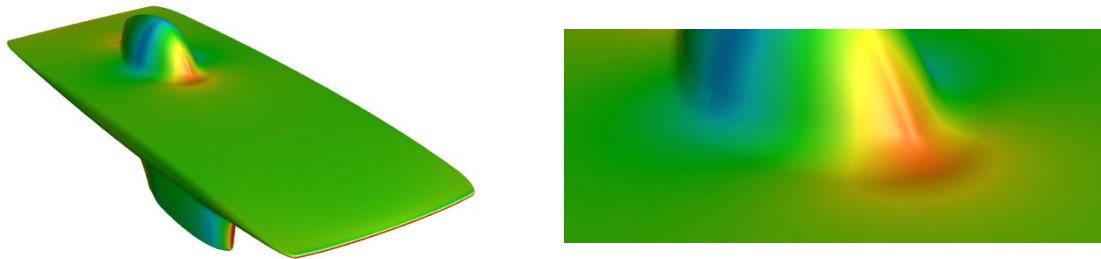


Figure 15. Pressure distribution on Solaris 7 with a camera.

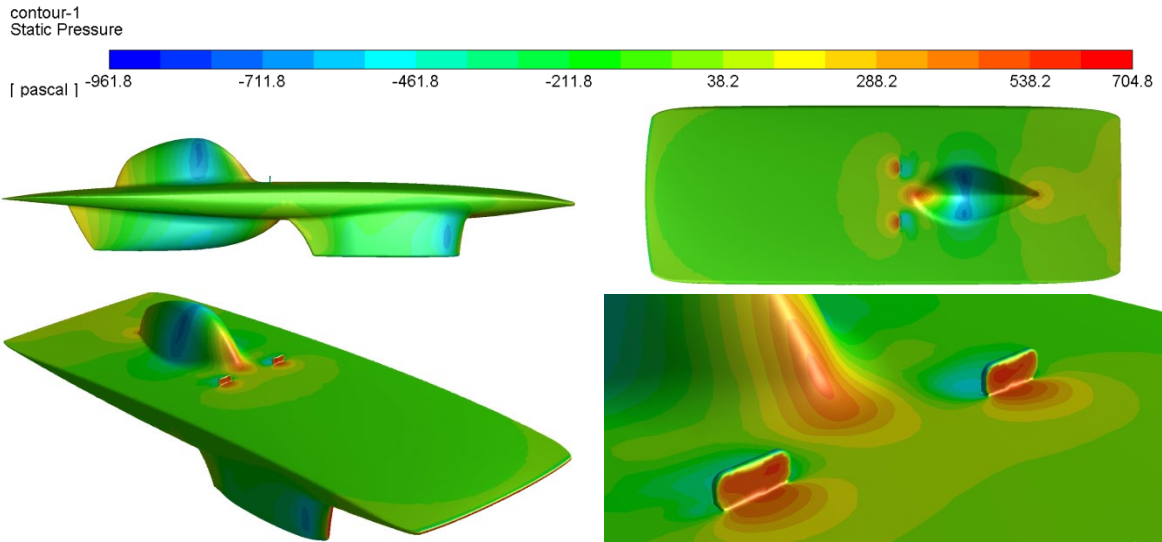


Figure 16. Pressure distribution on Solaris 7 with mirror.

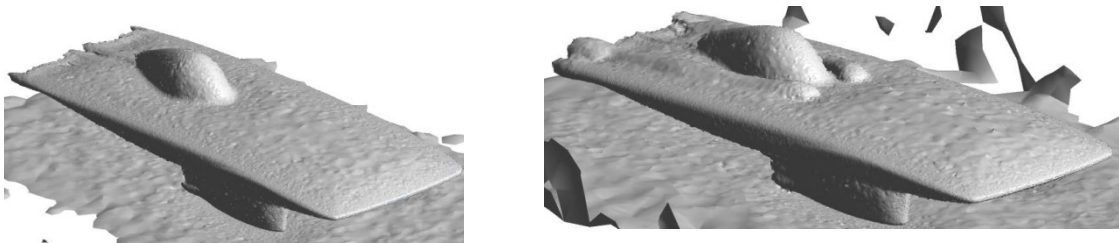


Figure 17. Vortex core regions.

CONCLUSION

In this study, the flow structures of Demobil 09 EV and Solaris 7 solar car and aerodynamic forces acting on both vehicles were investigated and determined numerically. The effects of a back-view camera and wing mirrors were analysed. The aerodynamic structures of vehicles were analysed under various yaw angles. According to the numerical results, using wing mirror on Demobil 09 EV increased the drag coefficient by 20.42% and the back-view camera on electric vehicle increased the drag coefficient by 5.37%. Using wing mirrors on Solaris 7 solar car increased the drag coefficient by %42 and the back-view camera on Solaris 7 solar car increased the drag coefficient by 23.72%.

Consequently, using the back-view camera on electric vehicle 15.05% more efficient. Using the back-view camera on solar car 18.28% more efficient. Therefore, the back-view camera is preferred to wing mirrors for improving the aerodynamics structure of vehicles. The pressure distribution of the electric vehicle has been found to be unbalanced around the wing mirrors and in the connection between the roof and the windshield. A sudden pressure drop was observed at the roof and wheel areas of the electric vehicle. It has been determined that sudden changes in the pressure distribution cause the drag coefficient to increase. The slant angle should be narrower in order to reduce the aerodynamic drag. The aerodynamic improvements can be obtained by covering vehicle wheels.

In addition to pressure drop, the drag coefficient increases with increasing yaw angle between 0 and 60°. Drag coefficients are increased by 52.13%, 194.43%, 569.14% and 783.09% with increasing each 15° of yaw angle. This case for solar car is 140.81%, 772.36%, 2684.76% and 7467.14%.

In the present study, aerodynamic structures of solar and electric vehicles were examined. It has been obtained that the use of a back-view camera is more efficient and drag coefficients increased with increasing each 15° of yaw angles.

When all these circumstances take into consideration, we could determine that yaw angle have a significant effect on power consumption for the race strategy. For future work it is advisable to look additionally into aeroacoustics, more extensive soiling investigation.

ACKNOWLEDGEMENT

Authors would like to thank M. Akif Ezan and S9 Solaris Team members for their help in the implementation of Computational Fluid Dynamics analysis and performing tests.

REFERENCES

- [1] Osawa H, Nishikawa S, Higashida D. Development of aerodynamics for a solar race car. *JSAE Review* 1998; 19(4): 343-349.
- [2] Wahba EM, Al-Marzooqi H, Shaath M, Shahin M, El-Dhmarshawy T. Aerodynamic drag reduction for ground vehicles using lateral guide vanes. *CFD Letters* 2012; 4(2): 68-79.
- [3] Chowdhury H, Moria H, Ali A, Khan I, Alam F, Watkins S. A study on aerodynamic drag of a semi-trailer truck. *Procedia Engineering* 2013; 56(2013): 201-205.
- [4] Bello-Millán FJ, Mäkelä T, Parras L, Del Pino C, Ferrera C. Experimental study on Ahmed's body drag coefficient for different yaw angles. *Journal of Wind Engineering and Industrial Aerodynamics* 2016; 157(2016): 140-144.
- [5] Gören A. Solar Energy Harvesting in Electro Mobility. In: Bizon N, Tabatabaei NM, Blaabjerg F, Kurt E, editors. *Energy harvesting and energy efficiency: technology, methods, and applications*: Springer, Cham, 2017, p 293-326.
- [6] Taherkhani AR, Gilkeson C, Gaskell P, Hewson R, Toropov V, Rezaenia A, Thompson H. Aerodynamic CFD based optimisation of police car using bezier curves. *SAE INT. j. Mater. Manf.* 2017; 10(2): 85-93.
- [7] Ahmad NE, Abo-Serie E, Gaylard A. Mesh Optimization for ground vehicle aerodynamics. *CFD Letters* 2010; 2(1): 54-65.
- [8] Desai M, Channiwala SA, Nagarsheth HJ. A comparative assessment of two experimental methods for aerodynamic performance evaluation of a car. *Journal of scientific and industrial research* 2008; 67(7): 518-522.
- [9] Lokhande BS, Sovani S, Khalighi B. Transient Simulation of the Flow Field Around a Generic Pickup Truck. In: *SAE 2003 World Congress & Exhibition, Detroit, Michigan, United States of America, 2003.*
- [10] Hu, X., & Wong, E. T. T. A numerical study on rear-spoiler of passenger vehicle. *World Academy of Science, Engineering and Technology (WASET)* 2011; no 57, p. 636-641; 2011.
- [11] Bayındırlı C, Akansu Y, Salman MS, Çolak D. The numerical investigation of aerodynamic structures of truck and trailer combinations. *International Journal of Automotive Engineering and Technologies* 2015; 4(3): 139-145.
- [12] Thacher EF. *A Solar Car Primer: A guide to the design and construction of solar-powered racing vehicles*. 1st ed. Springer; 2015.
- [13] Altinisik A, Yemenici O, Umur H. Aerodynamic analysis of a passenger car at yaw angle and two-vehicle platoon. *Journal of Fluids Engineering* 2015; 137(12)/ 121107.
- [14] Korkut TB, Gören A, Ezan MA. A CFD study on photovoltaic performance investigation of a solar racing car. In: Dincer I, Colpan CO, Ezan ME, editors. *Environmentally-Benign Energy Solutions*: Springer, Cham, 2020, p 509-529.
- [15] Kayansayan N, Alptekin E, Ezan MA. Thermal analysis of airflow inside a refrigerated container 2017; Volume 84, Pages 76-91
- [16] Korkut TB, Gören A, Ezan MA. Photovoltaic panel efficiency modeling for solar powered vehicle. In: *7th Global Conference on Global Warming, Izmir, Turkey; 24-28 June, 2018.*
- [17] Amromin EL. Vehicles drag reduction with control of critical reynolds number. *ASME Journal of Fluids Engineering* 2013; 135(10): 101-105.
- [18] Mokhtar WA. Aerodynamics of high-lift wings with ground effect for racecars. *SAE Technical Paper No. 2008-01-0656.*
- [19] Howell JP. Shape features which influence crosswind sensitivity. *Proceedings of the Institution of Mechanical Engineers* 1993; Part E, 9, pp. 43-52.
- [20] Mieller, C. Lockheed Georgia low speed wind tunnel Honda Civic hatchback airtab modification results. *Lockheed Georgia Company Wind Tunnel Test 2002 No. 561.*
- [21] Ahmad NE, Abo-Serie E, Gaylard A. Mesh optimization for ground vehicle aerodynamics. *CFD Letters* 2010; 2(1): 54-65.
- [22] Kumar CR, Chowdary JU, Reddy KA. Study of aerodynamic drag reduction using vortex generators. *International Journal of Advanced Engineering Sciences and Technologies* 2011; 7(10): 181-183.
- [23] Jones B. *Elements of practical aerodynamics*. 3th Edition: Wiley; 1942.
- [24] Carroll DR. *The winning solar car : A design guide for solar race car teams*. Society of Automotive Engineers; illustrated edition; 2003.
- [25] Good L, MG, Garry KP. On the use of reference models in automotive aerodynamics. *SAE Technical Paper 2004-01-1308*
- [26] Ljungberg J. CFD and aerodynamics at Volvo car corporation. Retrieved from https://www.mech.kth.se/courses/5C1211/Externals_2011/Ljungberg2.pdf; March 2011.
- [27] Meteorology A. Coober Pedy, South Australia October 2017 Daily Weather Observations. Retrieved from <http://www.bom.gov.au/climate/dwo/201710/pdf/IDCJDW5012.201710.pdf>; 2017.

- [28] Fluent. Continuity and momentum equations. Retrieved from <https://www.sharcnet.ca/Software/Fluent6/html/ug/-node382.htm>; 2006.
- [29] SAS. Standard k-epsilon model. Retrieved from https://www.sharcnet.ca/Software/Ansys/16.2.3/enus/help/-flu_th/flu_th_sec_turb_ke.html; 2016.
- [30] Korkut TB, Gören A, Ozaydın O, Armakan E. Aerodynamic effects of composite wheel cover on electric vehicle (EV) (Part B). *Putech & Composite* 2019; 7(3): 16-20.
- [31] Karimi Sadaghiyani O, Soufi Boubakran M, Hassanzadeh A. Energy and exergy analysis of parabolic trough collectors. *International Journal of Heat and Technology*, 2018; 36(1): 147-158.
- [32] Olsson M. Designing and optimizing side-view mirrors. department of applied mechanics, Division of Vehicle Engineering and Autonomous Systems, Chalmers University of Technology
- [33] Yemenici O. An experimental investigation of the flow over an automobile side rear view mirror. *International Journal of Mechanical and Production Engineering (IJMPE)* 2017;5(9): 52-54.